Initial performance of the attitude control and aspect determination sub-systems on the *Chandra* Observatory

Robert A. Cameron[a], Thomas L. Aldcroft[a], William A. Podgorski[a], Mark D. Freeman[a], Jeffrey J. Shirer[b]

[a]Harvard-Smithsonian Center for Astrophysics, [b]TRW Space & Electronics Group, 60 Garden Street, Cambridge, Massachusetts 02138, USA

ABSTRACT

The pointing control and aspect determination (PCAD) subsystem of the *Chandra* X-ray Observatory plays a key role in realizing the full potential of *Chandra's* X-ray optics and detectors. We review the performance of the spacecraft hardware components and sub-systems, which provide information for both real time control of the attitude and attitude stability of the *Chandra* Observatory and also for more accurate *post-facto* attitude reconstruction. These flight components are comprised of the aspect camera (star tracker) and inertial reference units (gyros), plus the fiducial lights and fiducial transfer optics which provide an alignment null reference system for the science instruments and X-ray optics, together with associated thermal and structural components. Key performance measures will be presented for aspect camera focal plane data, gyro performance both during stable pointing and during maneuvers, alignment stability and mechanism repeatability.

Keywords: aspect, Chandra, spacecraft, optics

1. INTRODUCTION

The *Chandra* Observatory has a pointing control and aspect determination (PCAD) subsystem which provides hardware and algorithms to perform in-flight attitude determination, pointing control, slewing and momentum management. In addition to the real-time control of the observatory, the PCAD subsystem also includes hardware and functionality to generate additional telemetry data, which is used in more accurate aspect determination of the science instrument data in *post-facto* ground processing. The observatory spacecraft, including the PCAD subsystem, was manufactured by TRW Space & Electronics.

This paper will primarily address those aspects of the subsystem performance related to the real-time operation of the observatory during the science mission and its ability to meet the goals of the science mission. Other subsystem functions, such as operation during perigee transits when science data are not being collected, backup safe-mode operations and solar-array pointing, will be discussed only briefly. A companion paper (Ref. 1) describes the *post-facto* aspect determination system and its performance.

The subsystem used during the science mission consists of the following sensors, actuators and optics, with associated electronics and support structures:

Aspect Camera Assembly (ACA) 11.2 cm optical telescope, stray light shade, two CCD detectors (primary and redundant) and two sets of electronics. The ACA can track up to 8 images simultaneously.

Inertial Reference Units (IRU) Two IRUs, each containing two 2-axis, rate-integrating, strapdown gyroscopes. Normal operation has one IRU running, providing data in 4 axes.

Fiducial Light Assemblies (FLA) LEDs mounted around each science instrument (SI) detector which are imaged in the ACA via the fiducial transfer system.

Further author information: (Send correspondence to R.A.C.)
R.A.C.: E-mail: rcameron@cfa.harvard.edu
T.L.A.: E-mail: taldcroft@cfa.harvard.edu
W.A.P.: E-mail: wpodgorski@cfa.harvard.edu
M.D.F.: E-mail: mfreeman@cfa.harvard.edu
J.J.S.: E-mail: jshirer@cfa.harvard.edu

Fiducial Transfer System (FTS) Consists of the retro-reflector collimator (RRC, a corner cube plus collimating lens) mounted at the center of the X-ray optics, and a periscope. The FTS collimates the light from the FLAs and directs it to the ACA, via the retro-reflector and periscope.

Fine Sun Sensor (FSS) A digital sun sensor with a $\pm 50^{\circ} \times \pm 50^{\circ}$ field of view and 0.02° resolution.

Coarse Sun Sensor (CSS) Four analog sensors mounted at the outer corners of the *Chandra* solar panels, providing a combined 4π steradian field of view.

Reaction Wheel Assembly (RWA) Six reaction wheels, mounted in a pyramidal configuration. Each RWA can provide 20 in-oz of control torque and 60-ft-lb-sec of momentum storage at bi-directional speeds up to 6000 rpm. Normal operation uses all 6 RWAs.

Momentum Unloading Propulsion System (MUPS) Thrusters used to unload momentum from the RWAs.

The key performance requirements for the PCAD subsystem are shown in Table 1. In general terms, the celestial pointing requirements apply to the real-time pointing control of the observatory, while the aspect determination requirements apply to the *post-facto* analysis.

Table 1. Key performance requirements for the PCAD subsystem

Requirement Type	Description	Requirement Measure	Requirement (arcsec)
Celestial Pointing	Absolute Pointing	Radius (99%)	30.0
	Pointing Stability	RMS half-cone angle in 95% of all 10-second intervals	0.25
Aspect Determination	Image Reconstruction	Diameter spread (rms)	0.5
	Celestial Location	Radius (rms)	1.0

Figure 1 shows the layout of the optical components of the PCAD subsystem. The IRUs are also mounted on support structure attached to the telescope optical bench, to ensure alignment stability to the telescope and PCAD optical components. The PCAD subsystem has two principal operating modes for the science mission: normal point mode and normal maneuver mode. In normal point mode, used for science observations, the observatory is controlled on a fixed inertial attitude. The on-board pointing control software combines star positions from the ACA and angle data from the IRU in a Kalman filter to estimate the attitude and attitude errors, and to produce a continuous update of the bias drift rates in the gyros. The RWAs provide control torques. In normal maneuver mode, the observatory is slewed between science targets using the IRUs to provide attitude and rate data, and the RWAs provide control torques. To protect the x-ray detectors from over-exposure to bright x-ray sources in normal point mode, the pointing direction of the observatory is continuously dithered, in the shape of a small Lissajous pattern on the sky.

In normal operation, the ACA tracks both stars and fiducial lights: typically 5 stars and 3 fid lights. Only the star data are used for the real-time pointing control of the observatory. The angular coordinate system in the ACA field of view is the fundamental coordinate system for real-time pointing control of the observatory.

For the *post-facto* aspect determination, the star positions and fid light positions from the ACA constitute a null-reference measurement system. Celestial location is determined by the angular separation between the star positions and the fid light positions: the fid light positions map the x-ray detector coordinate system and x-ray photons onto the celestial sphere. A boresight observation of a known x-ray field was performed early in the science mission to initially define the coordinate system mapping for each x-ray detector. Image reconstruction uses the angular differences between successive measurements of the stars and fid lights to register x-ray photons in the same location.

In the following sections, the performance of overall PCAD subsystem is described, together with a discussion of some issues that have arisen in the operation of the PCAD subsystem. This is followed by discussion of the performance of individual PCAD sub-assemblies.

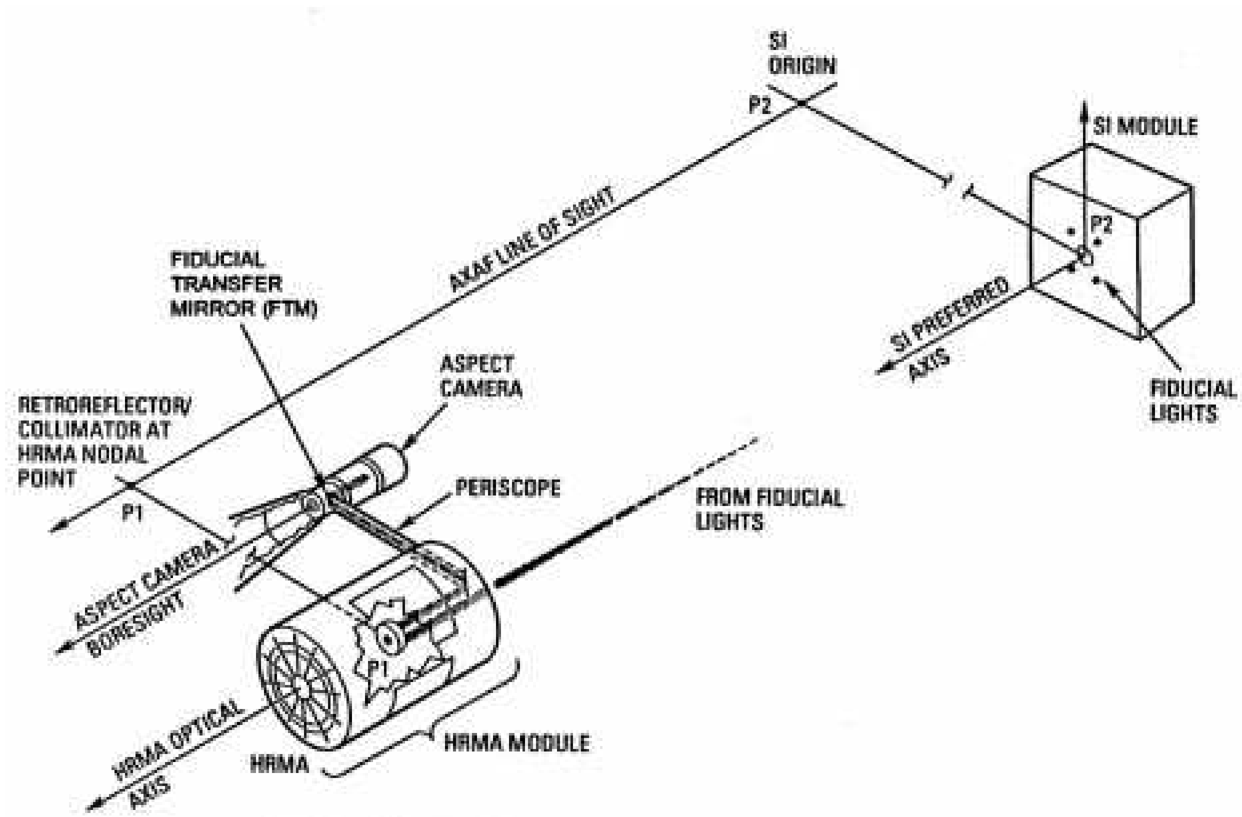

Figure 1. Optical components of the Pointing Control and Aspect Determination subsystem.

2. SUBSYSTEM PERFORMANCE

2.1. Pointing Accuracy

The two performance requirements for celestial pointing accuracy given in Table 1 are both met by *Chandra*.

Absolute celestial pointing refers to the accuracy with which the *Chandra* line of sight (the line connecting the nominal x-ray detector aim-point and the HRMA node) can be pointed toward a location on the sky. From a small sample of ACIS observations, the 99% limit on absolute celestial pointing is about 3 arcsec radius, well within the requirement. Ref. 1 describes the time history of the celestial location accuracy of *Chandra*, as determined from the history of deviations from the initial boresight calibrations of the x-ray detectors. The observed shift in the observatory boresight also contributes to the absolute celestial pointing error, but is also small, about 2 arcseconds.

Pointing stability over the time period November 1999 to January 2000 is shown in Figure 2. For each day in this period, the time spent in normal pointing was split into 10-second intervals, and the absolute pointing error in pitch and yaw were calculated for each interval. The pitch and yaw errors were quadrature summed to give the total absolute pointing errors. Figure 2 shows the daily averages of the absolute pointing error, and also the 95th-percentile absolute pointing error. The daily averages include attitude errors at the start of observations, when maneuver errors are settling out, and during perigee passages, when gravity-gradient disturbance torques are maximum. It can be seen that the PCAD pointing stability, which is the dominant contributor to the observatory pointing stability, is well below the observatory requirement of 0.25 arcsecond given in Table 1. Reaction wheel momentum dumping causes pointing disturbances of as much as 30 arcseconds, over timescales of a few minutes. To date, momentum dumping has been performed during maneuvers and not during science observations.

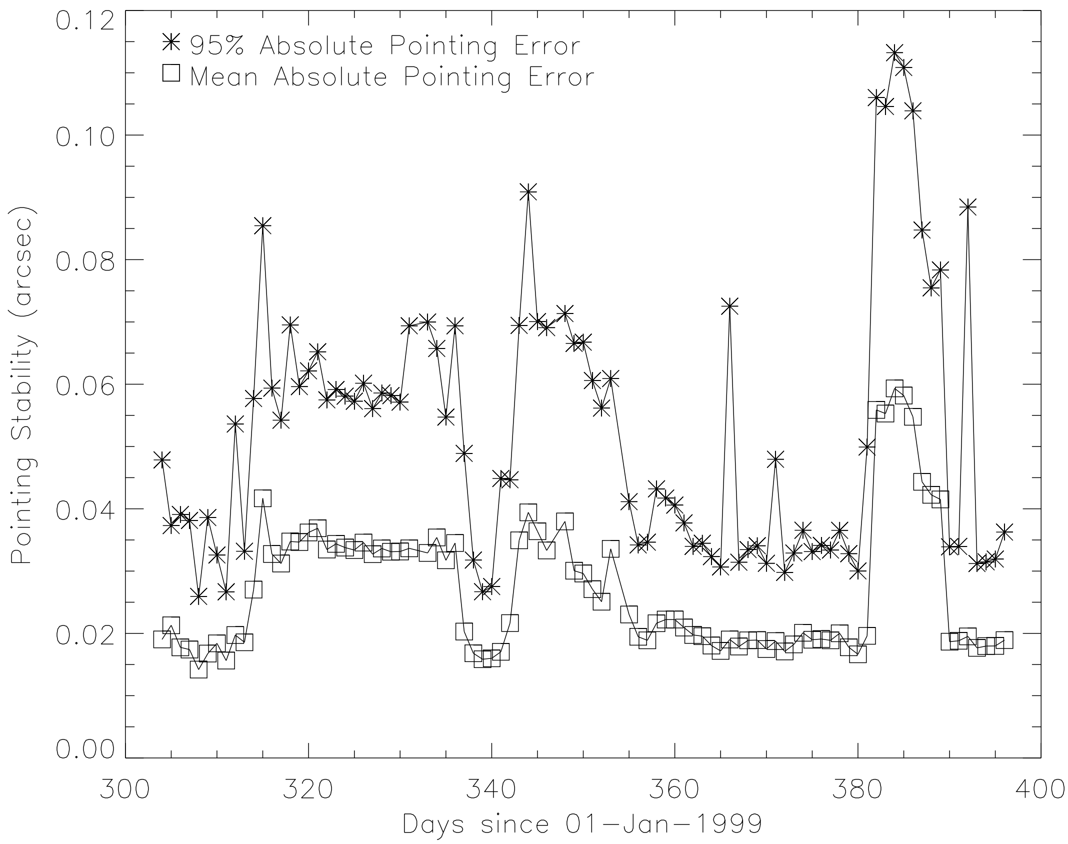

Figure 2. Pointing Errors, November 1999 - January 2000. The mean absolute pointing error, and the pointing error of 95% of 10 second intervals are shown for each day.

The largest pointing errors and pointing instability occur in January 2000, between day 382 and 389 in Figure 2. This time period corresponds to a period of changed behaviour in gyro 2 in the primary IRU. During this time period, the operating current drawn by gyro 2 increased from 103 mA to $\sim$ 110 mA, with an accompanying change in the pitch and yaw bias drift rates and increased noise in bias rates. The gyro current returned to its normal value on day 389. Similar changes in the gyro 2 operation occurred in December 1999. The gyro 2 operation will be discussed more fully in section 3.2.

2.2. Maneuver Accuracy

For this discussion, maneuver accuracy is defined as the difference between the expected and actual celestial locations at the end of a maneuver. This is an important performance measure, since *Chandra* must correctly locate its position on the sky at the end of each maneuver. If it cannot, then the pre-programmed sequence of science observations cannot be continued, and observations are halted until the Flight Operations Team re-establishes the attitude of the observatory and rebuilds and reloads a revised observing sequence. The PCAD subsystem uses a very limited catalog of 3 to 5 "acquisition" stars for each observation to establish its pointing direction at the end of each maneuver. Once a successful pattern match is found, a "one-shot" attitude update is performed, to remove the residual pointing error at the end of the maneuver before the science observation starts.

Figure 3 shows the magnitude of residual pointing errors at the ends of maneuvers performed from November 1999 to January 2000. Also shown is the curve of limiting maneuver error allowed for in observation planning. There is no obvious trend of error versus time, although the maneuvers which reach the limit of the allowed error all occur in mid-December, when there was a period of bias variability in gyro 2. Maneuver errors have several contributors:

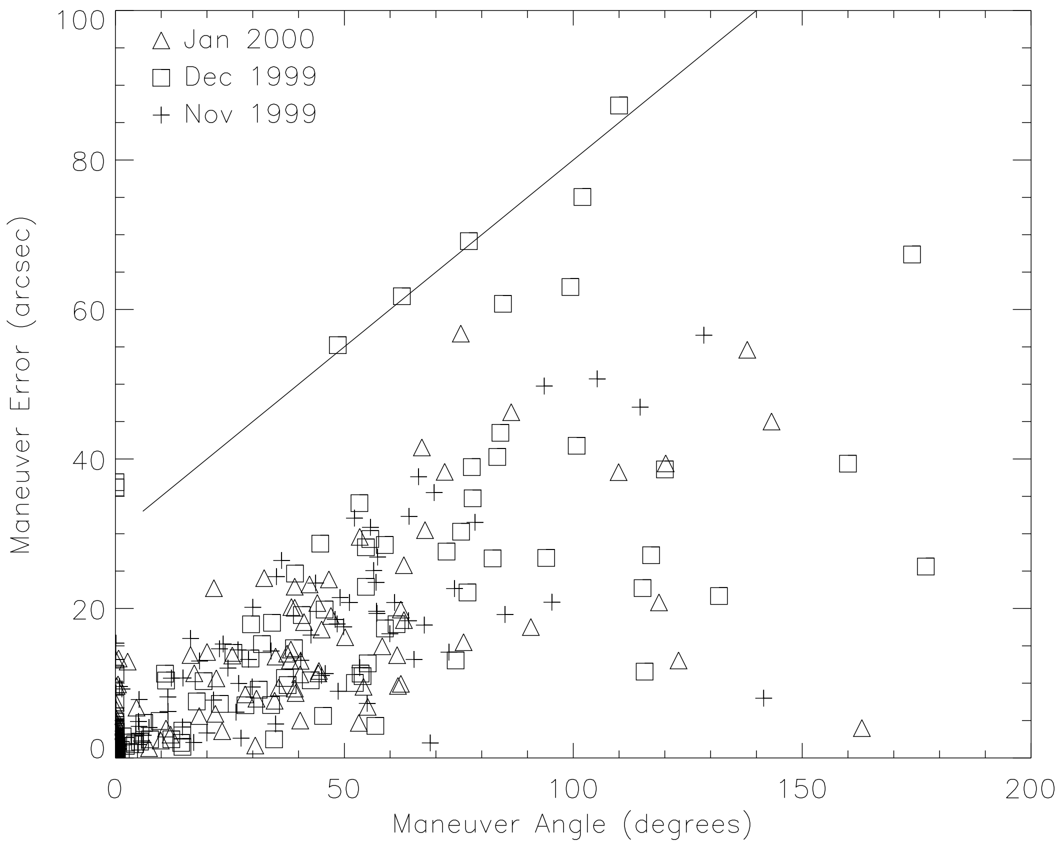

Figure 3. Maneuver Errors, November 1999 - January 2000. Residual pointing errors at the end of maneuvers are shown for each month. The curve is the maneuver error limit used in planning searches for guide stars at the end of maneuvers.

errors in the gyro scale factors; errors in the alignments of the gyro axes; errors in the gyro drift rates; stellar aberration effects; star catalog errors; and initial roll errors propagating to final pitch and roll errors through the maneuver. The absence of a long-term trend suggests that the alignments and scale factors of the gyros are stable over this time-frame. Since the gyro drift rate estimates are continually updated by the Kalman filter in normal pointing, the drift rate variations have not been large enough or frequent enough to cause maneuver problems.

3. UNIT-LEVEL PERFORMANCE

3.1. Aspect Camera

The ACA[2] was manufactured by Ball Aerospace, and is an f/9 Ritchey-Chretien telescope with 990mm focal length. The ACA has a 1024×1024 pixel CCD focal plane, with a $1.4° \times 1.4°$ field of view, so that each pixel subtends approximately 5 arcsec. The ACA optics spread the energy from a star or fid light over about 4 pixels. The ACA electronics calculates the centroid of each image from an 8×8 pixel array using a first moment centroid in each axis. These centroids are used for on-board pointing control. Stars in the magnitude range $V \simeq 6$ to 10.2 are selected as guide stars, and the fid lights are set at $V \simeq 7$. Figure 4 shows the commanded dither of the observatory for a 50000 second observation, and the ACA-generated centroid of a 9.6 magnitude star.

The first moment centroiding algorithm used by the ACA can be perturbed by warm pixels (*i.e.* pixels with higher than average dark current) near the star or fid light image. Figure 5 shows the effect a warm pixel which is dithered into the vicinity of a star during an observation. The total image brightness increases while the warm pixel

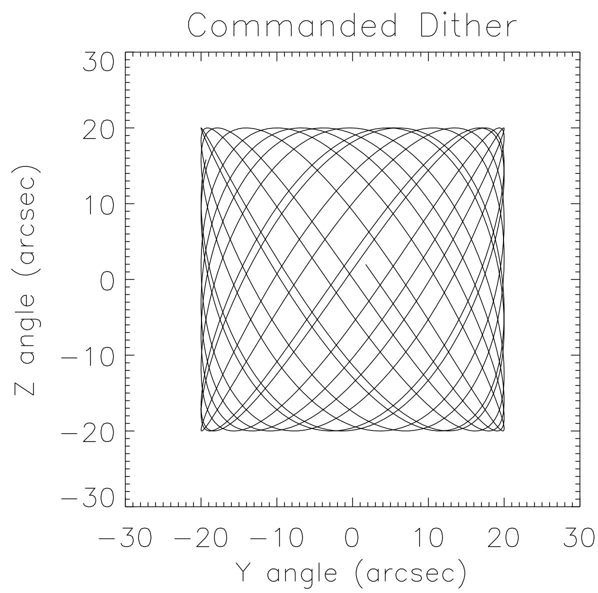

Figure 4. Observation Dither Pattern and ACA-generated centroid data for a magnitude 9.6 star.

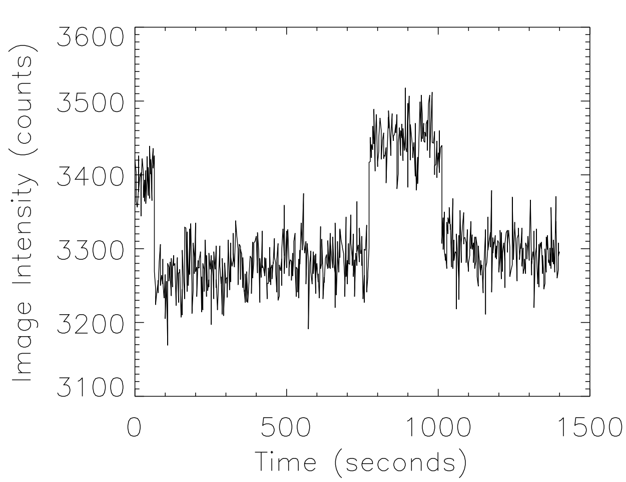

Figure 5. The effect of a warm pixel on image intensity and ACA-generated centroid. Pointing dithering brings the star image into the vicinity of a CCD pixel with high dark current, increasing the measured star brightness and perturbing the measured centroid.

of about 180 counts/second is in the image, and the centroid of the magnitude 9.6 star is perturbed by about 0.5 arcseconds. The pointing dither has been subtracted from the centroid data to show the effect of the warm pixel more clearly.

The effects of such star centroid perturbations are mitigated by the averaging of the centroid data for (typically) 5 guide stars. Such effects do not cause problems for the real-time pointing control of *Chandra*, as demonstrated by the observatory pointing accuracy discussed in the previous section. However, such effects also show the potential

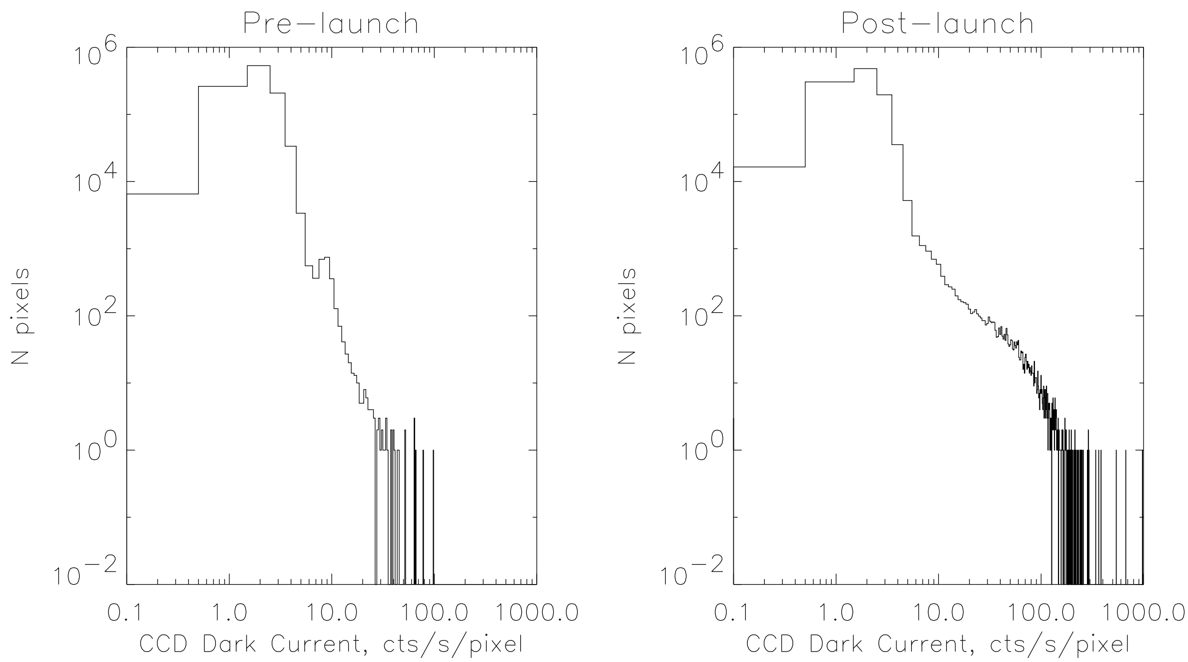

Figure 6. Histograms of the ACA CCD dark current per pixel, pre-launch and post-launch. The post-launch data were obtained 19 days after launch, and show a tail of dark current values extending to above 100 counts/s/pixel.

improvement that can be obtained in the *post-facto* aspect solution by using more sophisticated image centroiding techniques. Ground centroiding can also be improved by using accurate dark current maps for the ACA CCD detector to provide an accurate background subtraction in the image data before centroiding. The *Chandra* Science Operations Team plans to perform full-CCD calibrations of the ACA dark current periodically throughout the mission, as dictated by the analysis of residual aspect errors in ground processing.

Figure 6 shows the histograms of dark current for the full ACA CCD focal plane operating at –10 C, from pre-launch calibration and from an early in-flight calibration 19 days after launch, when *Chandra* had been boosted to its final operating orbit. Each dataset has been filtered to remove the effects of transient ionizing radiation. The post-launch histogram clearly shows the effects of particle radiation on the CCD, due to several passages through the Earth's radiation belts during the transfer orbit. The median dark current remains approximately constant at 1.9 counts/s/pixel, while the 99th-percentile dark current has risen from 4.2 counts/s/pixel to 5.4 counts/s/pixel. A small number of pixels have dark currents above 100 counts/s.

In addition to reporting positions, the ACA also provides instrumental magnitude data to the on-board computer, to further ensure stars tracked by the ACA during an observation match the preloaded star catalog for the observation. The photometric calibration of the reported ACA magnitudes has been improved since launch from observations of stars with known V magnitudes and $B - V$ colours. An revised guide star catalog with improved colour transformations to the ACA instrumental system has been produced. This provides almost 100% success in the acquisition and tracking of guide stars during the mission.

The images of stars and fiducial lights being tracked by the ACA are occasionally perturbed by deposited charge from ionizing particle radiation hitting the ACA CCD. This can cause the image centroid calculated by the ACA to be displaced so that the ACA loses track of the image. The PCAD software in the on-board computer can recognize this situation for the stars begin tracked, and re-issue a search command to the ACA to re-acquire the lost star. The PCAD software does not do this for fiducial light images. Consequently, a software patch was prepared for the ACA processor by Ball Aerospace, which limits the allowed angle change between successive centroid calculations for fiducial lights. This software update was uploaded to the ACA in September 1999, and has successfully prevented loss of track of the fiducial lights.

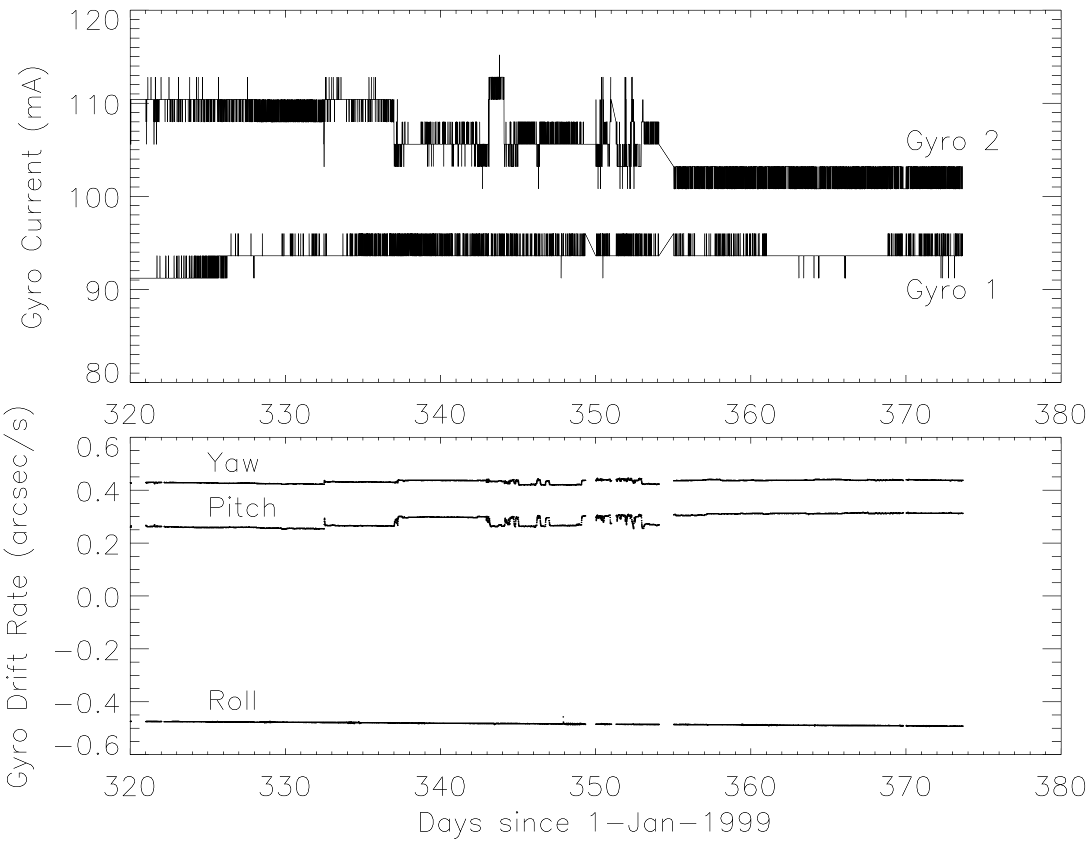

Figure 7. IRU-A gyro motor currents and estimated drift rates. The top plot shows the current drawn by each gyro over several weeks of operation. The bottom plot shows the variation in the estimated gyro drift rates, corresponding to the current variation in gyro 2.

3.2. Inertial Reference Units

Each IRU contains two gyros, manufactured by Kearfott based on the SKIRU V design. Each gyro provides angle data in two orthogonal axes. The resultant 4 axes of data allow a consistency check on the gyro operation. Data from the gyros are transformed to the spacecraft roll, pitch and yaw axes for use by the PCAD pointing control software. Gyro drift rates estimates are generated in the roll, pitch and yaw axes by the Kalman filter. Presently, only IRU-A is being used for the normal science mission.

Performance of the gyros has been within requirements since the start of the mission. A small variation in the current drawn by each gyro has been noticed. Gyro 1 has shown a gradual increase in current from $\sim$ 89 mA to $\sim$ 94 mA. Gyro 2 has shown more irregular variations in current. Gyro 2 current is typically 103 mA, but shows occasional jumps to larger values, typically about 110 mA, but as high as 125 mA. These current jumps are accompanied by a change in the gyro drift rates, with a sensitivity of about 0.002 deg/hour/mA. In addition, the bias measurements become slightly more noisy. There is a resultant increased variation in torque commands to the reaction wheels, with a resultant degradation in the real-time pointing stability of *Chandra* that was discussed in the analysis of sub-system performance. The measured drift rate sensitivity is similar to other SKIRU gyros, and comparable gyro current changes have been seen in similar gyros on other missions. Figure 7 shows the gyro motor currents and the gyro drift rates estimated by the Kalman filter between late 1999 and early 2000. The current changes in gyro 2 mostly affect pitch and yaw bias rates. The more sophisticated ground aspect processing shows no obvious problem during these episodes.

3.3. Fiducial Transfer System

The FTS and the x-ray telescope were manufactured by Eastman Kodak. The FTS consists of passive optical components mounted to the x-ray telescope. Its performance depends on the mechanical stability of its various components, and on the thermal stability and thermal control of the associated support structures. While the purpose of the FTS is to reduce alignment sensitivity in the aspect solution, excessive alignment shifts could cause problems. An important diagnostic of the FTS performance is the variation of measured fid light positions in the ACA field of view. This measures the variation of the alignments of various components:

- the fiducial lights to the x-ray detectors
- the x-ray detectors to the Science Instrument Module (SIM)
- the SIM to the optical bench on which the x-ray telescope and SIM are mounted
- the x-ray optics to the optical bench
- the internal alignment of the FTS periscope
- the ACA mount to the x-ray telescope
- the ACA to the ACA mount.

These alignments are temperature sensitive. Temperature variations provide insight into the alignment shifts of individual components, via the observed correlations between temperature changes and changes in observed fid light positions. An example of such temperature-based alignment shifts is shown in Figure 8.

The SIM is mounted to the optical bench on 3 focus-adjust flexures. One of these mount points is on the –Z (sun-facing) side of the optical bench. This flexure is heated by direct sunlight when the observatory is at sun pitch angles less than 90 degrees. Figure 8 shows the temperatures of the three SIM flexures after a maneuver which brought the –Z flexure into sunlight. Also shown are the changes in the Y and Z angles of a fid light during the same time period, with a 0.5 arcsecond shift in the Z angle over several hours.

In the list of alignments given above, all but two alignments are continuously compensated for in the *post-facto* aspect solution. Two alignment shifts that are not nulled out are alignment shifts of the fiducial lights relative to the x-ray detectors, and relative tilt alignment shifts between the two fold mirrors in the FTS periscope. Alignment shifts between the fiducial lights and the x-ray detectors can produce celestial local errors if the fiducial lights move, and celestial location and absolute pointing errors if the x-ray detectors move. Tilts between the two fold mirrors in the FTS periscope will produce celestial location errors. As discussed in Section 2, the absolute pointing of *Chandra* is well within requirements. Celestial location errors are discussed in Ref 1.

Fiducial light positions are stable to within ~ 1 arcsecond over the timescales of observations. The longer-term stability of the FTS and measured fid light positions is affected by such factors as long-term temperature changes and the repeatability of the SIM mechanisms. Various parts of the optical bench and PCAD units have risen in temperature through the mission, as thermal blankets age. For example, the ACA housing temperature has risen about 1° C. The FTS periscope, a key component of the FTS system, has shown no significant change in overall temperature or temperature gradients along and across the periscope, suggesting little alignment shift within the periscope.

3.4. Science Instrument Module

The Science Instrument Module[3] was manufactured by Ball Aerospace. It houses the two X-ray detectors, and provides 2-axis mechanical adjustment to translate either detector into the telescope aim-point and to adjust the focus of the detectors. Thus the repeatability of the SIM mechanisms is closely related to the real-time performance of the x-ray telescope and detectors. The positioning of the SIM in translation and focus is controlled by a 3-phase brushless DC motor with commutation control by Hall sensors mounted on the motor shaft. The translation table moves on three linear bearings, and is driven by a ball nut riding on a ball screw driven by the translation motor. Reference positions for each mechanism are provided by reference tabs, which pass optical sensors mounted on the support stage. Comparison of the actual and expected Hall sensor step counts at each tab crossing provides an independent measure of the repeatability of each mechanism.

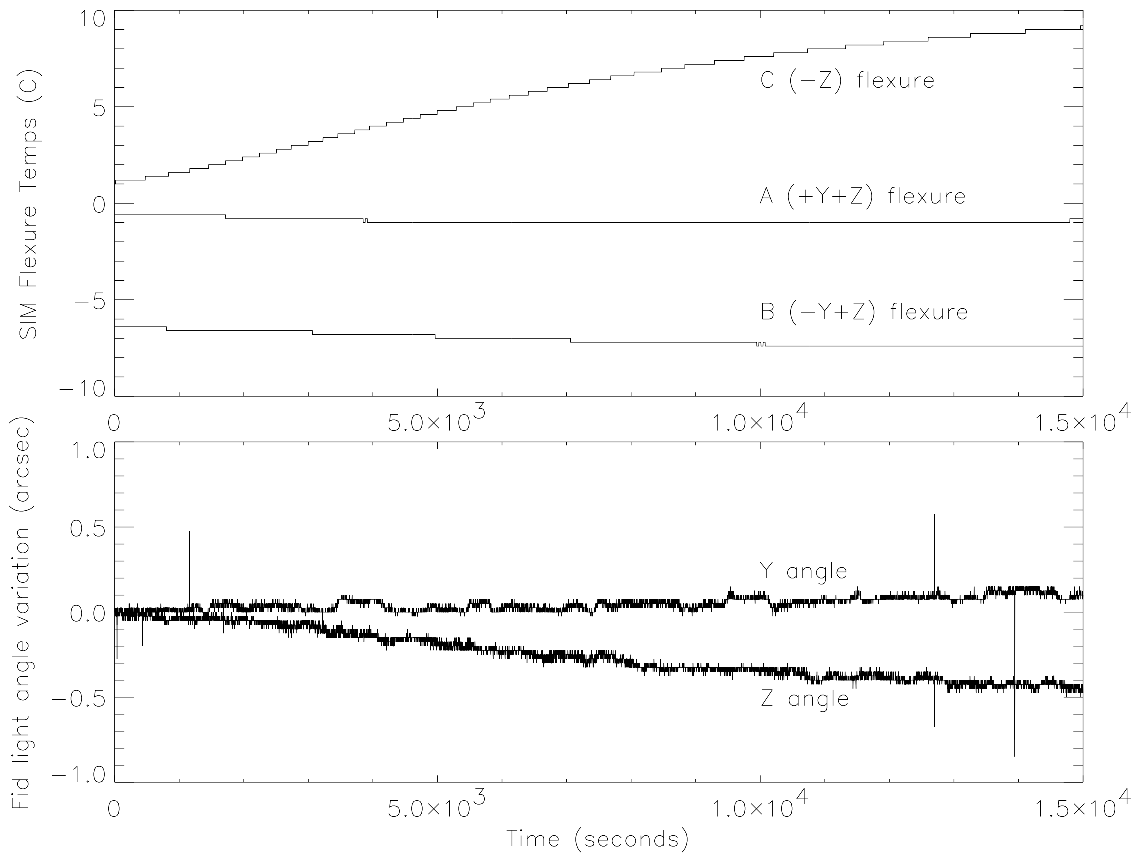

Figure 8. SIM flexure temperature changes and fid light position changes. The top plot shows the change in SIM temperatures following a pitch maneuver. The bottom plot shows the change in the observed position of a fiducial light measured by the ACA, where the Z angle changes as the SIM –Z flexure heats up.

Figure 9 shows the repeatability of the translation table, as measured at each of three reference tab positions. The scatter in the tab positions meets the performance requirements of the SIM. Tab 2 is used to update the position knowledge of the SIM. Tab 2 position measurements have a maximum variation of 44 steps (0.1 mm) which corresponds to 2.3 arcseconds of variation at the x-ray detector focal planes. Certainly some of this variation can be attributed to uncertainty in the measurement of the tab position. Also shown in Figure 9 is the expected offset range for each tab, predicted from pre-launch testing. No trend in the tab offsets with time has been detected, indicating stable long-term operation of the SIM.

ACKNOWLEDGMENTS

The authors would like to thank Eric Martin and other members of the *Chandra* Flight Operations Team for helpful insights into the operation of Chandra, and for the successful operation of the science mission. David Morris has provided assistance and data analysis, and the data products of the CXC monitoring and trends group have provided valuable insight into *Chandra*'s long-term performance.

RAC, TLA, WAP, MDF and JJS were supported by the *Chandra* X-ray Center NASA contract NAS8-39073 during the course of this study.

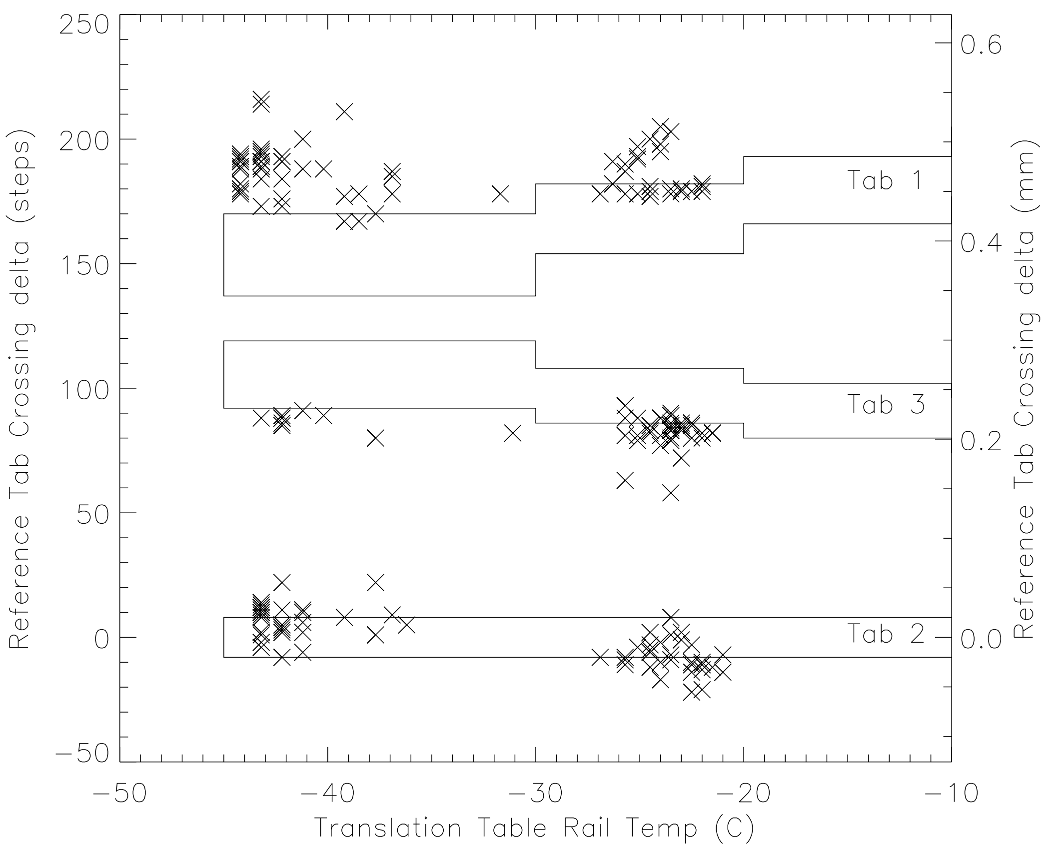

Figure 9. SIM translation table position repeatability. The difference between expected and measured translation table motor step count is plotted at each of three reference tab positions on the translation table. One translation step = 0.00215 mm. The boxes represent the range of each tab predicted from pre-launch testing.

REFERENCES

1. T. Aldcroft, M. Karovska, M. Cresitello-Dittmar, R. Cameron, and M. Markevitch, "Initial performance of the aspect system on the chandra observatory: Post-facto aspect reconstruction," in *Astronomical Telescopes and Instrumentation 2000*, J. Truemper and B. Aschenbach, eds., *Proc. SPIE* **4012**, 2000.
2. D. L. Michaels, "Performance of the aspect camera assembly for the advanced x-ray astrophysics facility," in *Acquisition, Tracking, and Pointing XII*, M. K. Masten and L. A. Stockum, eds., *Proc. SPIE* **3365**, pp. 232–241, 1998.
3. M. A. Skinner and S. P. Jordan, "AXAF: the science instrument module," in *EUV, X-Ray, and Gamma-Ray Instrumentation for Astronomy VIII*, O. H. Siegmund and M. A. Gummin, eds., *Proc. SPIE* **3114**, pp. 2–10, 1997.